Journal of Applied Electrochemistry **29**: 561–568, 1999.

Reaction of CO/CO_2 gas mixtures on Ni–YSZ cermet electrodes

P. HOLTAPPELS[1]*, L. G. J. DE HAART[1], U. STIMMING[1‡], I. C. VINKE[1] and M. MOGENSEN[2]
[1]*Institut für Werkstoffe und Verfahren der Energietechnik, Institut 3: Energieverfahrenstechnik, Forschungszentrum Jülich, 52425 Jülich, Germany;*
[2]*Materials Research Department, Risø National Laboratory, PO Box 49, DK-4000 Roskilde, Denmark*
*(*author for correspondence, e-mail: peter.holtappels@risoe.dk; present address: Materials Research Department, Risø National Laboratory, PO Box 49, DK-4000 Roskilde, Denmark)*

Received 20 May 1998; accepted in revised form 11 September 1998

Key words: carbon monoxide oxidation, solid oxide fuel cells, unstable reaction rate

Abstract

The reaction of carbon monoxide/carbon dioxide mixtures on Ni–YSZ cermet electrodes was investigated as a function of the electrode potential and the partial pressures of the reactants at 1273 K. Time-dependent reaction rates are observed for the CO oxidation reaction for oxygen activities corresponding to open circuit potentials in the range from −750 to −1010 mV. The electrode changes between a passive state and several active states for the CO/CO_2 reaction. Periodic changes of the reaction rate for the CO oxidation are observed every 30 and 80 s. The impedance spectra recorded at the rest potential and the overpotential dependence of the CO oxidation rate indicate a change in the number of active sites in the reaction zone. In the active state, the CO oxidation reaction is more than one order of magnitude slower than the hydrogen oxidation reaction on these Ni–YSZ cermet electrodes. These results indicate clear differences in the kinetics of the CO and H_2 oxidation reaction.

1. Introduction

Solid oxide fuel cell (SOFC) systems are attractive for energy conversion because they can be directly fed with carbon containing fuels like natural gas or coal gas. This is possible because at temperatures above 873 K natural gas in the presence of water vapour can be reformed into a mixture of hydrogen, water, carbon monoxide and carbon dioxide. The H_2 and CO thus produced are oxidized in the SOFC. The electrochemical oxidation of H_2 proceeds at the interface electrolyte–electrode which, in case of the SOFC, are yttria stabilized zirconia (YSZ) and a Ni–YSZ cermet, respectively. Numerous investigations of the electrochemical behaviour of H_2/H_2O mixtures on Ni–YSZ cermet electrodes have been conducted and are still in progress.

Mogensen et al. [1] investigated the influence of the microstructure on the electrode performance for the H_2/H_2O reaction. From these results an influence of the cermet structure in a complicated manner is indicated. Divisek et al. [2] concluded that elementary reaction steps like charge transfer and adsorption control the H_2 oxidation rate on Ni–YSZ cermet electrodes. From these observations it is evident that the surface structure at the electrode/electrolyte interface is important for the electrode performance. The oxidation of CO on Ni–YSZ cermet electrodes has also been investigated [3–5]. The results of these investigations are, however, not conclusive.

The aim of this work was to study the electrode kinetics of the $CO|CO_2||Ni–YSZ|YSZ$ system and to compare it to the hydrogen oxidation on a well-known Ni–YSZ cermet anode. The experimental part was carried out using the high performance Ni–YSZ cermet anodes, developed at the Risø National Laboratory, Materials Research Department. These anodes have already been investigated under H_2/H_2O gas atmospheres [6].

2. Experimental details

Most of the Ni–YSZ cermet anodes were prepared by wet powder spraying [7] on pressed and sintered YSZ

pellets, specially designed at Risø for single electrode measurements [8]. The electrode area was 0.44 cm^2. A schematic diagram of the measurement cell is shown in Figure 1. Pt, painted on the side of the YSZ–electrolyte which was exposed to air, acted as cathode. The fuel compartment was sealed using a gold ring. Ni–YSZ cermet anodes prepared on YSZ pellets were heated at 5 K min^{-1} up to 1273 K, the anode compartment being flushed with Ar. Subsequently, the anode was reduced at this temperature under 97% H_2/3% H_2O atmospheres (humidified hydrogen). Electrochemical measurements were carried out in CO/CO_2 atmospheres. For reference, additional measurements were performed under H_2/H_2O atmospheres.

Due to the Boudouard reaction (1),

$$2\,CO \rightarrow C + CO_2 \tag{1}$$

that is favoured by high CO/CO_2 ratios and low temperatures [9, 10] carbon can be deposited in the anode. This may lead to destruction or poisoning of the anode. To avoid this effect, the CO/CO_2 ratios were kept below the value of 20.

A second cause of damage of the Ni–YSZ cermet anode is NiO formation at high oxygen activities. The critical $a(O_2)$ for the NiO formation at various temperatures can be calculated from an Ellingham diagram [11]. For the equilibrium:

$$CO + \tfrac{1}{2}\,O_2 \rightleftharpoons CO_2 \tag{2}$$

the oxygen activity in a CO/CO_2 mixture can be calculated from the Gibbs free energy [9]:

$$\Delta G^0_{f,T} = -282.5 + 0.0866\,T \tag{3}$$

where $\Delta G^0_{f,T}$ is in kJ mol^{-1}.

To avoid both carbon deposition and NiO formation, the used CO/CO_2 ratios, $p(CO)/p(CO_2)$, ranged from 0.2 to 20. Different CO and CO_2 partial pressures were obtained by mixing CO (grades 2.0 or 5.6), CO_2 (4.5) and Ar (5.0) from gas bottles using Brooks 5878 mass flow controllers. On Ni–YSZ cermet anodes prepared on pellets, impedance spectroscopy at open circuit potential, quasisteady state current voltage measurements and chrono amperometry measurements at constant applied potential were performed using a 1280 Schlumberger electrochemical measurement system controlled by a personal computer and the FCL software package [12]. The temperature was measured at the sample before each measurement using an HP3421 data acquisition control unit controlled by the FCL computer code. The temperature at the Ni–YSZ cermet electrode was controlled within 1 K. The impedance measurements are analysed using the EQUIVCRT program [13].

Additionally Ni–YSZ cermets were prepared in a similar manner to that described above; annular shaped electrode geometries (4–12 mm dia.; area 1 cm^2) on tape cast electrolyte foils (Kerafol) were produced. A sketch of the test cell is given in Figure 2. The Ni–YSZ cermet anodes were heated in Ar with 2 K min^{-1} up to 1273 K and subsequently reduced at this temperature in 20% H_2/3% H_2O. On these samples electrochemical measurements were performed using a Bank LB81 laboratory potentiostat in combination with a Solartron 1255 FRA. Results obtained on Ni–YSZ cermet anodes prepared and measured on tape cast electrolyte foils are indicated in the text. Results obtained on Ni–YSZ cermet anodes prepared on electrolyte pellets (Fig. 1) are not especially marked.

After the electrochemical experiments the samples were microscopically investigated.

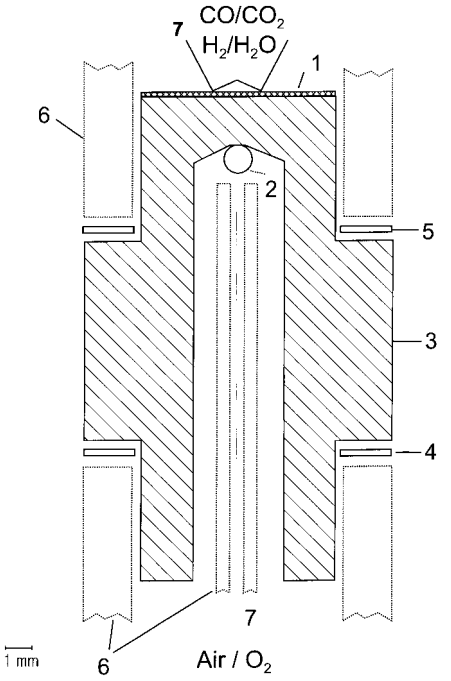

Fig. 1. Schematic diagram of the measurement cell using pressed and sintered YSZ pellet: (1) Ni–YSZ cermet electrode; (2) Pt point reference electrode; (3) YSZ pellet; (4) Pt counter electrode; (5) Au seal; (6) Al_2O_3 tubes; (7) Pt wire.

3. Results

A representative micrograph of the cross section of a Ni–YSZ cermet electrode is shown in Figure 3. This sample was exposed to CO/CO_2/Ar (0.1/0.02/0.88) at

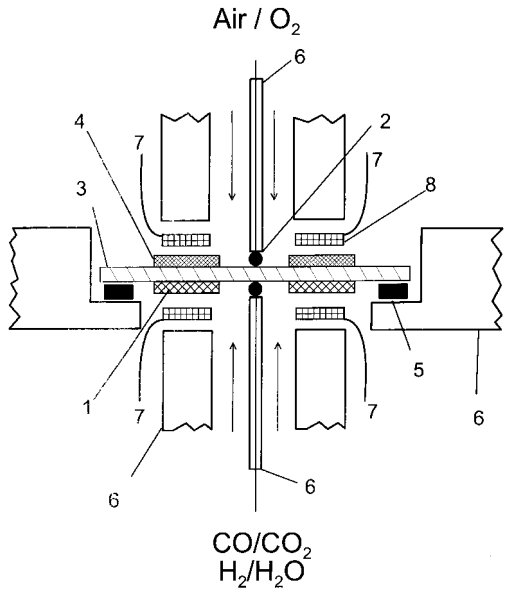

Fig. 2. Schematic diagram of the measurement cell using tape cast YSZ foils: (1) Ni–YSZ cermet electrode; (2) Pt point reference electrode; (3) YSZ tape; (4) Pt counter electrode; (5) Au seal; (6) Al_2O_3 tubes; (7) Pt wire; (8) Pt mesh.

1273 K for 24 h. Areas different in grey scale can be distinguished in the picture. The light areas are the metallic Ni phase. The medium grey areas are the ceramic YSZ phase. Pores filled with embedding material give dark areas. A uniform distribution of all three phases is observed in the micrograph. Maximum and minimum grain sizes are estimated from the micrograph to be 3 and 0.5 μm, respectively. The pore size is of the same order of magnitude. Similar structures were observed for Ni–YSZ cermet electrodes investigated in H_2/H_2O only, and for samples investigated both in various CO/CO_2 and in H_2/H_2O atmospheres.

Initial impedance measurements and quasi steady state current voltage curves measured after changing the atmosphere to CO/CO_2 mixtures indicate a highly unstable electrode reaction. Reverting H_2/H_2O atmospheres eliminates this instability.

An example of the current time response for CO oxidation at constant applied potential of -900 mV vs Pt/air (corresponding to a polarization of 40 mV including the ohmic loss in the electrolyte) is given in Figure 4. The time between each data point is 50 s. At the start of polarisation, the current is below the detection limit of the system. During this period the electrode is considered as passive for the CO oxidation reaction. After 2.5 min the Ni–YSZ cermet electrode becomes active for the CO oxidation reaction. Subsequently the current density decreases within 10 min from 4.3 to 1.7 mA cm^{-2}. Longer active and passive periods were also observed in which it was possible to obtain stable current voltage curves, and to perform impedance measurements.

Two quasisteady state current–overpotential curves (IR_Ω-corrected) for the CO oxidation reaction are given in Figure 5. Both measurements were performed at the same sample, under equal experimental conditions ($p(CO) = 0.2 \times 10^5$ Pa, $p(CO_2) = 0.02 \times 10^5$ Pa) at 1273 K. The lower current–overpotential curve is related to the passive electrode state, whereas the upper curve represents an active electrode state for the CO oxidation reaction. The passive state curve yields around 0.12 mA cm^{-2} at 200 mV anodic overpotential. The active state curve reaches 10 mA cm^{-2} at the same overpotential. The scatter in the passive state current–overpotential curve is due to the resolution of the measurement system. For overpotentials above 150 mV both the active and the passive current–overpotential curves show an apparent Tafel behaviour. The apparent

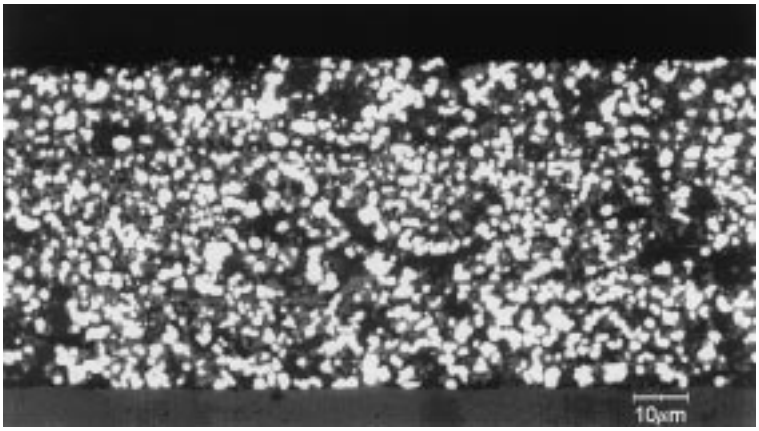

Fig. 3. Cross section of a representative Ni–YSZ cermet electrode after being exposed to CO/CO_2/Ar (0.1/0.02/0.88) at 1273 for 24 h.

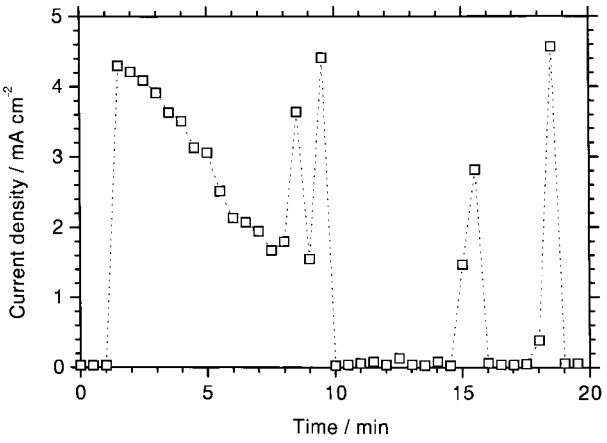

Fig. 4. Current density–time response of a Ni–YSZ cermet electrode at constant applied potential $\Delta U = -900\,\text{mV}$ vs Pt/air ($\Delta U_{OCV} = -940\,\text{mV}$), $p(CO) = 0.1 \times 10^5\,\text{Pa}$, $p(CO_2) = 0.02 \times 10^5\,\text{Pa}$, $T = 1273\,\text{K}$, electrode area $0.44\,\text{cm}^2$.

Tafel slopes are $275\,\text{mV} \pm 20\,\text{mV}$ and $355\,\text{mV} \pm 5\,\text{mV}$ for the passive and the active curve, respectively. The current density at overpotentials above 150 mV changes by a factor of 140 ± 20 between the two states.

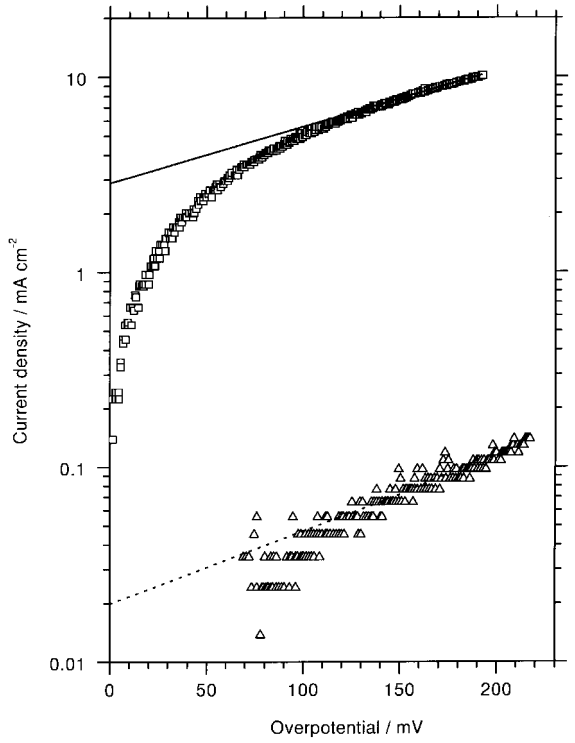

Fig. 5. Quasisteady state current potential curves at 1273 K; $p(CO) = 0.1 \times 10^5\,\text{Pa}$, $p(CO_2) = 0.02 \times 10^5\,\text{Pa}$, $p(Ar) = 0.88 \times 10^5\,\text{Pa}$. Symbols: (□) active electrode state, (△) passive electrode state; lines corresponding to slopes of $275\,\text{mV}\,\text{dec}^{-1}$ (· · · · ·) and $355\,\text{mV}/\,\text{dec}^{-1}$ (– – – –) are given for comparison. Electrode area $0.44\,\text{cm}^2$.

Figure 6 shows the impedance spectra measured at open circuit potential under the experimental conditions given above. A significant difference in the impedance is observed, indicating an active electrode state and the passive state.

For the active state, the Bode–Z_{im} plot (Fig. 6(a)) shows three time constants at 3 kHz, 2 Hz and 0.2 Hz. The impedance can be described by the equivalent circuit given in Figure 7(a), in which each time constant is represented by a resistor in parallel to a constant phase element (CPE). The ohmic resistance R_Ω is related to the ohmic drop in the YSZ electrolyte. Figure 6(b) shows the Nyquist plot for the active state and the simulation using this equivalent circuit. The high frequency semi circle is clearly depressed and the CPE can be replaced by a Warburg impedance. The Bode–Z_{im} plot in the passive state (Fig. 6(a)) shows only one maximum around 3 Hz. An equivalent circuit containing two time constants, as given in Figure 7(b), is necessary to describe the impedance in the frequency range from 4 kHz to 2 Hz. The higher and lower frequency sections in the passive electrode state could not be measured accurately. The Nyquist plot for the passive state compared to the simulation is given in Figure 6(c). In the high frequency part, the angle between the impedance and the real axis is nearly 45°. A Warburg element W in parallel to a resistor R_1 is used to describe this part of the impedance in both the active and the passive electrode state, suggesting a fast diffusion process in the reaction. The faradaic resistance related to the electrochemical reaction at the three phase boundary zone, R_{EC}, is given by the difference between the total resistance and the ohmic resistance R_Ω. In the passive electrode state, the faradaic resistance is around 140 times higher than in the active state. This value is in good agreement with the differences between the active and passive current densities at higher overpotentials in Figure 4.

Figure 8 shows the reciprocal faradaic resistance $1/R_{EC}$ as a function of the oxygen activity expressed as the potential difference vs Pt/air. Treating the CO/CO_2 mixture as an ideal gas, the change in the open circuit potential from -750 to $-1010\,\text{mV}$ corresponds to a change in $p(O_2)$ from 3×10^{-8} to $2 \times 10^{-12}\,\text{Pa}$. The graph shows two distinct regions. The passive state corresponds to $1/R_{EC}$ values below $0.009\,\text{S}\,\text{cm}^{-2}$. The active state ranges from 0.044 to $0.67\,\text{S}\,\text{cm}^{-2}$. The scatter of the points for the active state indicates a large number of semi stable electrode activities. This phenomenon seems to be independent of the oxygen activity.

The wide range of electrode resistances for the active Ni–YSZ cermet electrode should be reflected in the chrono amperometric measurements. Because the data

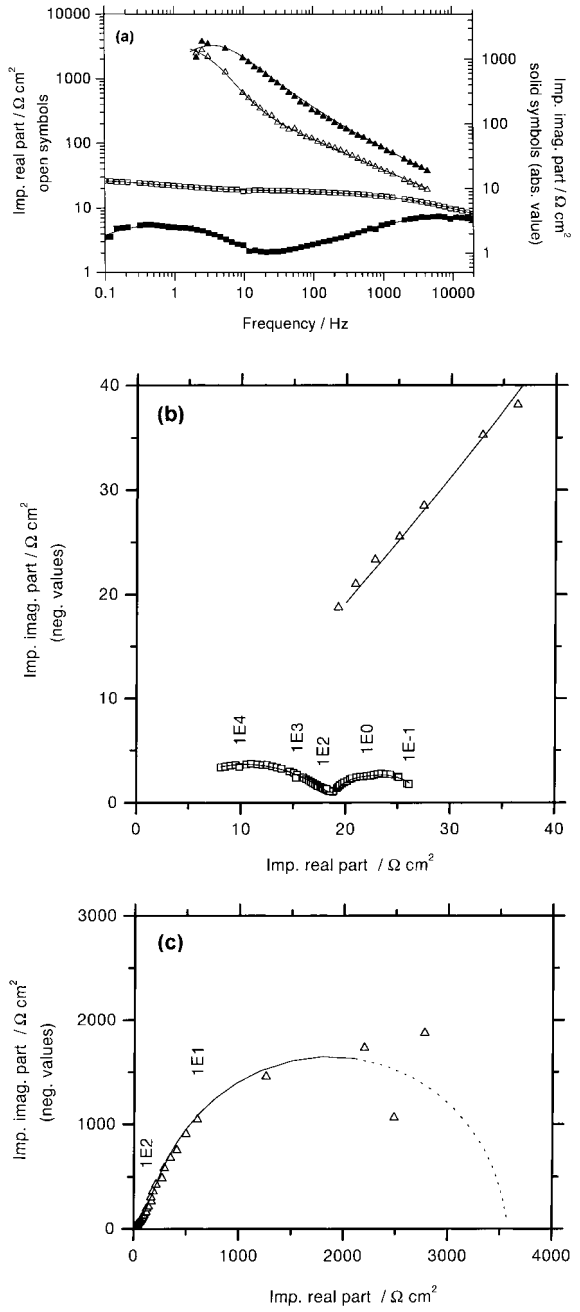

Fig. 6. Impedance spectra at open circuit potential at 1273 K; $p(CO) = 0.1 \times 10^5$ Pa, $p(CO_2) = 0.02 \times 10^5$ Pa; (a) Bode–Z_{real} and Bode–Z_{im} plot for active electrode state (□, ■) and passive electrode state (△, ▲); (b) Nyquist plots for the active electrode state (□); (c) Nyquist plot for the passive electrode state (△); lines represent the simulation using the equivalent circuits (Figure 7). Electrode area 0.44 cm^2.

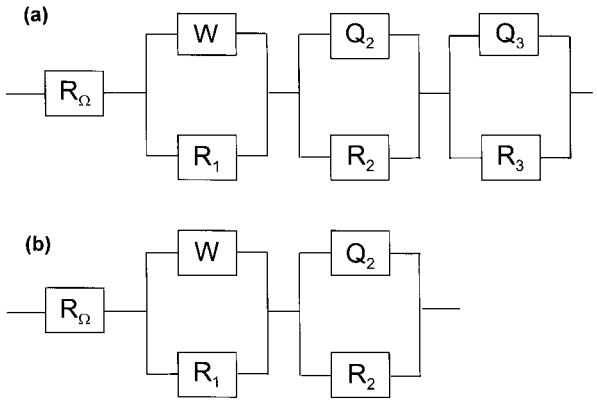

Fig. 7. Equivalent circuit describing the impedance spectra from 20 kHz to 0.1 Hz in the active electrode state (a), and from 4 kHz to 2 Hz in the passive electrode state (b).

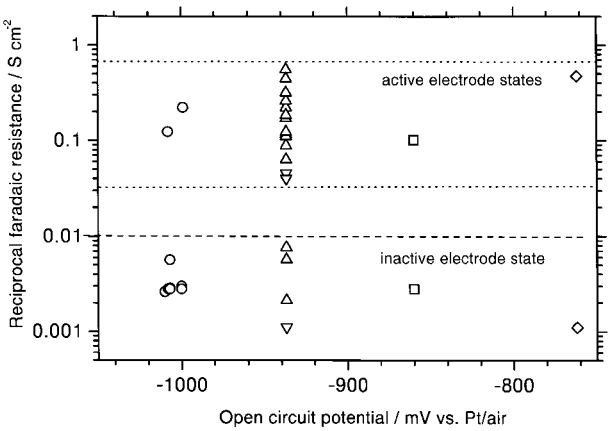

Fig. 8. Reciprocal faradaic resistance at 1273 K, obtained from impedance spectra and from current–potential curves at polarization ≤ 20 mV vs OCV. Key: (○) $p(CO) = 0.95 \times 10^5$ Pa, $p(CO_2) = 0.05 \times 10^5$ Pa, $\Delta U_0 = -1011$ mV vs Pt/air; (△) $p(CO) = 0.83 \times 10^5$ Pa, $p(CO_2) = 0.17 \times 10^5$ Pa, $\Delta U_0 = -938$ mV vs Pt/air; (▽) $p(CO) = 0.1 \times 10^5$ Pa, $p(CO_2) = 0.02 \times 10^5$ Pa, $\Delta U_0 = -938$ mV vs Pt/air; (□) $p(CO) = 0.06 \times 10^5$ Pa, $p(CO_2) = 0.07 \times 10^5$ Pa, $\Delta U_0 = -860$ mV vs Pt/air; (◇) $p(CO) = 0.17 \times 10^5$ Pa, $p(CO_2) = 0.83 \times 10^5$ Pa, $\Delta U_0 = -761$ mV vs Pt/air. Electrode area 0.44 cm^2.

presented in Figure 3 are obtained with a low time resolution, additional fast chrono amperometric measurements are performed. These fast chrono amperometric measurements were carried out on Ni–YSZ cermet electrodes prepared on tape cast electrolyte foils (see Fig. 2).

Figure 9 shows an example of the current time response, recorded with a sample rate of 10 points per second for $\Delta U = +50$ mV vs the rest potential for $p(CO) = 0.17 \times 10^5$ Pa and $p(CO_2) = 0.83 \times 10^5$ Pa at 1273 K. The measurement is started 4.5 h after the gas was changed from H_2/H_2O to CO/CO_2 atmospheres, and 2.5 h after beginning the polarization. The CO oxidation rate switches almost periodically between mainly three different electrode states. Two periodicities can be discerned. One process with a time constant in the

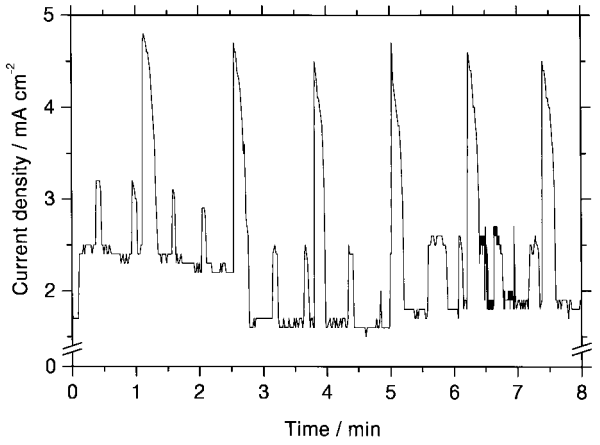

Fig. 9. Current density–time measurement at 1273 K at constant applied potential −700 mV vs Pt/air; 4.5 h after gas exchange from H_2/H_2O to CO/CO_2 and 2.5 h after beginning the polarisation; $p(CO) = 0.17 \times 10^5$ Pa, $p(CO_2) = 0.83 \times 10^5$ Pa, the measurement was carried out on an annular shaped Ni–YSZ cermet electrode prepared on a tape cast electrolyte foil. Electrode area 1 cm^2.

range 80–90 s instantaneously increases the current to a value of approximately 4.8 mA cm^{-2}, decaying within 20 s back to the initial value. A second process with a time constant around 30 s shows a pulse in the current density of 0.8 mA cm^{-2} with a duration of 5 s.

4. Discussion

The most prominent feature observed during the investigations of the CO oxidation reaction on the Ni–YSZ cermets is the time dependent reaction rate. The electrochemical characteristics for the active and the passive state of the CO oxidation show similar apparent Tafel slopes. This, combined with the fact that the time constants observed in the impedance measurements are almost the same, suggests a similar reaction mechanism for both states. The difference in activity can be tentatively attributed to a change in the number of active reaction sites. This is in agreement with an increase in the faradaic resistance at the open circuit potential by a factor 140 and a decrease in the current density at high overpotentials by a similar factor.

The phenomena of unstable reaction rates are reported for the heterogeneous catalysed CO oxidation reaction on Pt, for polycrystalline and single crystal catalysts as well as for supported catalysts [14–16]. In contrast to the heterogeneous catalysed CO oxidation reaction the oxygen involved in the anodic oxidation of CO in an SOFC is provided electrochemically, this means from oxygen ions in the electrolyte. Yentekakis and Vayenas [17] showed that the oscillating behaviour of the heterogeneous catalysed CO oxidation on Pt can also be controlled by the electrochemically pumped oxygen and, thus, by the electrochemical potential of the Pt catalyst. In SOFC, using Pt electrodes, periodically changing reaction rates have previously been observed for the anodic oxidation of ammonia [18].

In the literature three models are discussed to explain the experimentally observed unstable behaviour of the heterogeneous oxidation of carbon monoxide on Pt catalysts. For the low pressure regime (~10–4 torr) Ertl et al. [16] formulated a reconstruction model for a clean Pt single crystal surface. A surface reconstruction occurs due to a change in CO coverage and the two different surface modifications are characterised by a pronounced difference in the sticking coefficient for oxygen. Sales, Turner and Maple [19] introduced an oxidation-reduction model. Evidence for the formation of PtO deactivating the catalyst was obtained from infrared spectroscopy studies. A third model introduced by Sundaresan et al. [20] explained the deactivation of the surface due to the presence of carbon atoms that block the active sites. The two latter models were used to explain long period oscillations of the CO oxidation rate for supported Pt catalysts at high pressures. All these models are, in principle, able to explain periodically changing reaction rates but also aperiodic and chaotic behaviour with periods ranging from seconds to hours.

The chosen conditions under which the experiments were performed on the Ni–YSZ cermets exclude both NiO formation and C deposition. However, this must not exclude the possibility that carbon or NiO may be formed on the surface due to a heterogeneous potential distribution in the electrode. Therefore a certain coverage of NiO or carbon on pronounced sites on the electrode surface cannot be excluded.

In the above described work unstable reaction rates are only observed in CO/CO_2 atmospheres. Furthermore, Ni as an excellent bondbreaker, can catalyse the dissociation of CO into O and C. Considering the low oxygen activity compared to the high CO activity at the Ni–YSZ cermet electrode, carbon deposition may take place under the given temperatures and partial pressures of the reactants. Because carbon deposition is considered as an autocatalytic reaction, a progressive growth of the carbon phase can be expected after initial carbon formation [21]. The formation of carbon, most likely on the Ni-surface, may decrease the number of available reaction sites for the electrochemical CO oxidation and thus decrease the CO oxidation rate.

Investigations of the carbon deposition on single crystal surfaces show significantly different carbon

activities on different crystallographic orientations [22]. It was observed that carbon was deposited on the Ni(1 1 1) modification whereas the Ni(1 0 0) and Ni(1 1 0) orientations remain almost free from carbon (uncovered), although C was thermodynamically stable.

Based on a reasonable potential for carbon formation and assuming that (a) Ni single crystal domains with significant differences in carbon activity are present in the Ni–YSZ cermet electrode, and (b) reconstruction between the different Ni-surface modifications is allowed, the observed unstable reaction rates of the electrochemical CO oxidation reaction can tentatively described by a 'modified reconstruction model', illustrated in Figure 10. In the active electrode state, high CO-oxidation rates can be expected on a Ni surface almost free from carbon. In the passive state, most of the available reaction sites for the CO oxidation (most likely on the Ni surface) are assumed to be blocked by carbon. A reactivation of the electrode can be considered if the surface reconstructs into a modification with a significantly lower sticking coefficient for carbon followed by desorption of the carbon layer. This increases the number of available reaction sites and, therefore, the electrochemical CO oxidation rate. The cycle is completed after a rearrangement of the Ni-surface into its initial modification (high carbon activity). Related to the reconstruction model proposed by Ertl et al., reconstruction and rearrangement of the Ni-surface are assumed to be allowed in the Ni–YSZ cermet electrode, and to take place depending on the degree of the carbon coverage on the Ni-surface. Observations of structural and chemical changes on Ni-catalysts surfaces after carbon deposition are taken as an indirect support of the described modified reconstruction model [22].

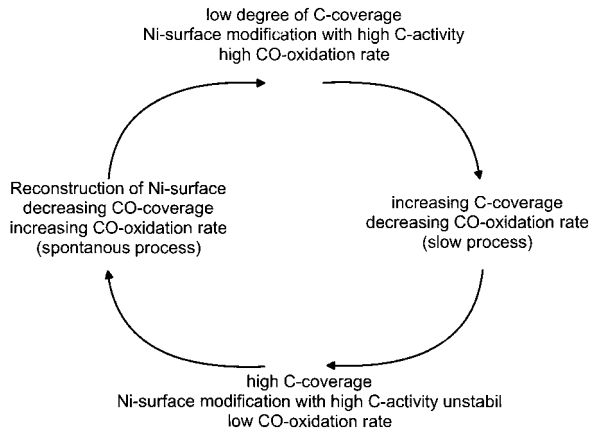

Fig. 10. Illustration of periodically changing CO oxidation rates, initiated by carbon deposition combined with reconstruction of the electrode surface.

From these results it is obvious that additional experiments are required in order to obtain insight into the processes taking place on Ni–YSZ cermet electrodes in CO/CO_2 atmospheres. Simultaneous monitoring of the CO_2 production (e.g. via online mass spectrometry) and in situ investigation of the catalyst surface using spectroscopic methods might give further information concerning the nature of the unstable electrochemical CO oxidation rate on the Ni–YSZ cermet electrodes investigated.

The CO oxidation on Ni–YSZ cermet electrodes was investigated by Aarberg et al. [5] as a function of the ratio CO/CO_2 and overpotential. The values given therein for $1/R_{EC}$, as well as the apparent Tafel-slopes, correspond well to the results presented in this work for the active electrode state. However, these workers reported no instabilities. This discrepancy, compared to the present work, is tentatively attributed to differences in the sample preparation, leading to different properties of the electrode surfaces.

For similar Ni–YSZ samples as were used in this study, Mogensen and Lindegaard [6] reported electrode resistances under H_2/H_2O atmospheres of $0.5\,\Omega$ (1273 K, $p(H_2) = 0.97 \times 10^5$ Pa, $p(H_2O) = 0.03 \times 10^5$ Pa) [6]. The CO oxidation at high CO concentrations and comparable $p(O_2)$ at 1273 K shows an electrode resistance of $10\,\Omega$. This shows that on these Ni–YSZ cermet anodes the hydrogen oxidation reaction is much faster then the CO oxidation reaction. Lower reaction rates for the CO-oxidation compared to the hydrogen oxidation were also reported by Kawada et al. [4] and Aarberg et al. [5]. The time dependent reaction rates observed for CO, have not been reported for the H_2 oxidation on Ni–YSZ cermets. The different reaction rates and the time dependence may suggest a fundamental difference in the reaction mechanisms for the hydrogen reaction and the carbon monoxide reaction on Ni–YSZ cermet electrodes.

As the shift reaction,

$$CO + H_2O \rightarrow CO_2 + H_2 \tag{4}$$

is fast at high temperatures it is most likely that, for fuels containing both H_2 and CO (i.e., reformer gas), the CO oxidation proceeds according to the shift reaction (Reaction 4) and not by the electrochemical oxidation reaction (Reaction 2).

5. Conclusions

It can be concluded that the observed multiple and periodically changing reaction rates are an intrinsic

property of the CO oxidation reaction on the Ni–YSZ cermet electrode. The origin of this change is believed to be related to the passivation and reactivation of active sites due to interactions between the CO/CO_2 atmosphere and the Ni–YSZ electrode surface. Although the detailed mechanism of the CO oxidation reaction is still unknown, the electrode processes are significantly different from the hydrogen oxidation reaction. Our results indicate clearly that more information concerning the submicrometric interface structure is required to understand the electrochemical processes on a gas exposed electrode surface at elevated temperatures.

Acknowledgements

This work was initiated in a cooperation between the Materials Research Department, Risø National Laboratory, Roskilde, Denmark and the Institut für Werkstoffe und Verfahren der Energietechnik Institut 3: Energieverfahrenstechnik, Forschungszentrum Jülich GmbH, Germany. The authors thank Jørgen Tyge Rheinländer for taking the optical microscope images. One of the authors (PH) would like to thank the Materials Research Department of the Risø National Laboratory, for giving him the opportunity to perform the work described here at Risø and Søren Primdahl for his support and fruitful discussions during his stay at Risø.

References

1. M. Mogensen, S. Primdahl, J.T. Rheinländer, S. Gormsen, S. Linderoth and M. Brown, Proceedings of the 4th International Symposium SOFC Yokohama, Japan, 1995, edited by M. Dokiya, O. Yamamoto, H. Tagawa and S. C. Singhal, **95-1,** (The Electrochem. Society, Pennington, NJ, 1995), p. 657.
2. J. Divisek, L.G.J. de Haart, P. Holtappels, U. Stimming and I.C. Vinke, Proceedings of the 17th Ris International Symposium on Materials Science: High temperature Electrochemistry: Ceramics and Metals edited by F.W. Poulsen, N. Bonanos, S. Linderoth, M. Mogensen, B. Zachau-Christiansen, (Ris National Laboratory, Roskilde, Denmark, 1996), p. 235.
3. T. Setoguchi, K. Okamoto, K. Eguchi and H. Arai, *J. Electrochem. Soc.* **139**(10) (1992) 2875.
4. T. Kawada, I. Anzai, N. Sakai, H. Yokokawa and M. Dokiya, Proceedings of the Symposium on High temperature Electrode Materials and Characterization edited by D. Macdonald, A.C. Khandkar, **91-6,** (The Electrochemical Society, Pennington NJ, 1991), p. 165
5. R.J. Aarberg, R. Tunold, S. Tjelle and R. degård, Proceedings 17th Ris *op cit*. [2], p. 511.
6. M. Mogensen and T. Lindegaard, Proceedings of the 3rd International Symposium on SOFC, Honolulu, Hawaii, 1993, edited by S.C. Singhal, H. Iwahara, **93-4,** (The Electrochem. Society, Pennington, NJ, 1993), p. 913.
7. C. Bagger, Fuel Cell Seminar, Tucson, AZ (1992), Program and Abstracts, p. 241.
8. J. Winkler, P.V. Hendriksen, N. Bonanos and M. Mogensen, *J. Electrochem. Soc.* **145** (1998) 1184.
9. U. Bossel, 'Facts and Figures', IEA SOFC Task Report, Bern (1992).
10. I. Barin, O. Knacke and D. Neuschütz, 'Thermodynamische Gleichgewichte bei der Erzeugung von Reduktionsgasen, Teil II: Das System C_{Sol}–H_2–CO–CO_2–H_2O–CH_4', Betriebsforschungsinstitut des Vereins deutscher Eisenhüttenleute, BFI-Bericht 166 (1971).
11. J.H.E. Jeffes, *J. Iron Steel Inst.* **160** (1948) 261.
12. B. Malmgren-Hansen, 'User Manual for FCL Software', Materials Department Ris (1991).
13. B.A. Boukamp, *Solid State Ionics* **20** (1986) 31.
14. L.F. Razon and R.A. Schmitz, *Catal. Rev.-Sci.-Eng.* **28**(1) (1986) 89–164.
15. F. Schüth, B.E. Henry and L.D. Schmidt, *Adv. Catal.* **39** (1993) 51–127.
16. R. Imbihl and G. Ertl, *Chem. Rev.* **95** (1995) 697–733.
17. I.V. Yentekakis and C.G. Vayenas, *J. Catal.* **111** (1988) 170.
18. R.D. Farr and C.G. Vayenas, *J. Electrochem. Soc.* **127** (1980) 1478.
19. B.C. Sales, J.E. Turner and M.B. Maple, *Surf. Sci.* **114** (1982) 381.
20. V.A. Burrows, S. Sundaresan, Y.J. Chabal and S.B. Christman, *ibid.* **180** (1987) 110–135.
21. L.C. Browning and P.H. Emmet, *J. Amer. Chem. Soc.* **74** (1952) 1680.
22. J.R. Rostrup-Nielsen, 'Steam Reforming Catalysis', Springer Verlag, Berlin/Heidelberg (1984).